Calibration Loop Antenna for Multiple Probe Antenna Measurement System

Yuming Zheng, *Student Member, IEEE*, Zibin Weng, *Member, IEEE*, Yihong Qi, *Senior Member, IEEE*,
Jun Fan, *Fellow, IEEE*, Fuhai Li, *Member, IEEE*, Zhiping Yang, *Senior Member, IEEE*,
and James L. Drewniak, *Fellow, IEEE*

Abstract—In order to achieve high accuracy in measurements of the multiple probe antenna measurement system (MPAMS), an omnidirectional calibration antenna with a small gain variation in the horizontal polarization (named calibration loop antenna, in convention) is required. This article presents such an antenna design. The proposed calibration loop antenna consists of four arc-folded dipoles with dimensions of 52 mm × 52 mm × 1 mm, balun structures for suppressing common mode current, and four parasitic strips for impedance matching on each of the top and bottom planes. The experimental results show that the proposed calibration loop antenna has a small gain variation in the horizontal polarization less than 0.16 dB in a bandwidth of 20% (2.25–2.75 GHz), and its 10-dB return loss bandwidth is 18.2%. Also, the cross-polarization ratio in the operating bandwidth is greater than 24 dB. Along with the desired omnidirectional radiation pattern, the low profile and compact design further make the proposed calibration loop antenna a suitable selection for calibration in MPAMS.

Index Terms—Balun, calibration antenna (CA), calibration loop antenna, common mode current suppression, gain ripple, horizontally polarized (HP), multiple probe antennas measurement system (MPAMS).

I. INTRODUCTION

WITH the rapid development of Internet of Things, over-the-air (OTA) performance of a wireless device is critical to the effective operation of a wireless network [1]–[5]. Compared with a single probe antenna measurement system that has to switch different measured orientations
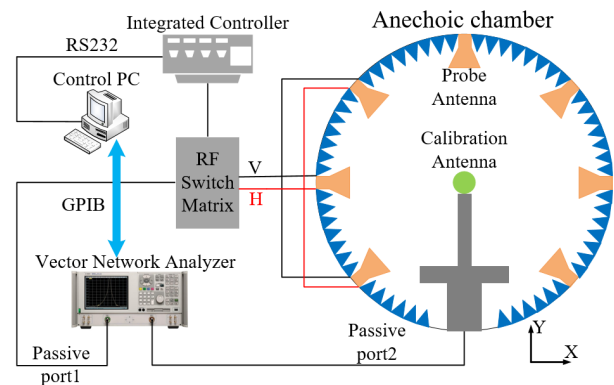
Fig. 1. Illustration of calibration of a typical MPAMS.

with mechanical rotation, a multiprobe antenna measurement system (MPAMS) has a higher measurement speed by using the electrical switch [6]. Thus, in today's OTA measurements [7], [8], MPAMS is widely used, where multiple probe antennas are designed to measure the radiation characteristics of the device under test (DUT) in different directions. However, because of the inconsistency of the absorbing materials combined with the difference in the gain of different probes, MPAMS requires calibration to ensure accuracy of the measurements. Fig. 1 illustrates the calibration process of a typical MPAMS. In the MPAMS, the probe antennas are placed in a ring, while the calibration antenna (CA) is placed in the center. The direction of the horizontal polarization is defined in parallel to the *xoy* plane, while the vertical polarization is in perpendicular to the *xoy* plane. Note that each probe antenna is a dual-polarized antenna consisting of both vertical and horizontal polarizations, thus the calibration must be performed for both polarizations. When calibrating in the vertical polarization direction, using only one dipole as the CA is acceptable, because the vertical polarization directions of all the probe antennas in the MPAMS are the same [9], [10]. However, since the horizontal polarization directions of the probe antennas in the MPAMS are different, it requires a horizontally polarized (HP) omnidirectional antenna as a HP CA for the MPAMS [11]. The gain variation in the horizontal polarization of the HP CA determines the accuracy of the calibration. Therefore, the HP omnidirectional antenna is required
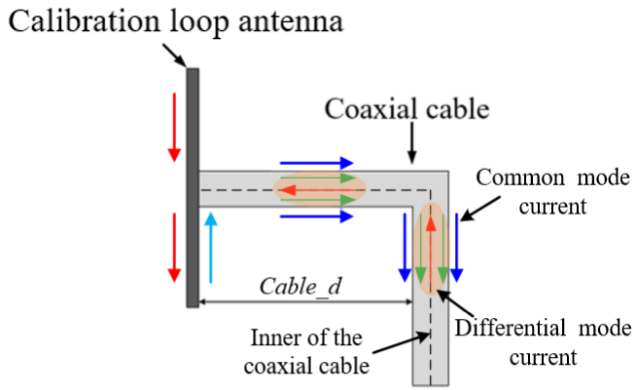
Calibration loop antenna

Fig. 2.   Effects of common-mode current on the calibration loop antenna.

to have a small gain ripple in the horizontal polarization. Such an antenna is called a calibration loop antenna.

According to the "test plan for 2×2 downlink multiple input and multiple output (MIMO) and transmit diversity OTA performance" specified by the Cellular Telecommunications and Internet Association (CTIA) [12], the gain ripple in the horizontal polarization of the calibration loop antenna for MPAMS must be less than 0.2 dB. However, for a calibration loop antenna without choking structures, part of the current on the calibration loop antenna will flow on the outer surface of the coaxial cable, resulting in common mode current. As shown in Fig. 2, horizontal common mode current vectors produce cross polarization and the vertical common mode current vectors produce the co-polarization component. The vertical common mode current at the bent part of the coaxial is superimposed on the radiation of the antenna, which changes the gain of the calibration loop antenna [13], [14] and then makes a larger gain ripple of the calibration loop antenna. Thus, if the *cable_d* illustrated in Fig. 2 changes, the gain ripple of the calibration loop antenna changes as well. This could result in several dBs of uncertainty during calibration [15]. Therefore, in order to have a small gain variation in the horizontal plane, the calibration loop antenna should suppress the common mode current (thus achieving a high cross-polarization ratio). At the same time, the trend for miniaturized anechoic chambers requires the calibration loop antenna to be small. Meeting all these requirements is very challenging, though highly desirable.

The classic calibration loop antennas, Alford loop antenna [16] and its derivatives, were first designed in 1940 and have been widely studied [17]–[19]. Alford loop antennas have a loop current distribution that forms an omni-directional radiation pattern by its unique structure. With this structure, the "Z"-type patches were printed on the dielectric board in [18], which was small and had a narrow operating bandwidth of 3.4%. In order to improve the bandwidth, many kinds of calibration loop antenna structures were proposed in recent years [20]–[29]. Among them, a planar antenna consisting of four pairs of flag-shaped radiators was designed in [27], covering the frequency band of 1.76–2.68 GHz with S11 < −10 dB. In [28], the use of parasitic strips resulted in an impedance matching bandwidth of 84%. However, the antenna

had large dimensions of $0.63\lambda_L \times 0.63\lambda_L \times 0.01\lambda_L$ (where λ_L is the free-space wavelength at the lowest frequency) and the gain variation in the horizontal plane was larger than 1.5 dB. In [29], a calibration loop antenna with planar folded dipole elements was presented, with 53.2% bandwidth and a small size of $0.34\lambda_L$. However, the gain ripple of the antenna was as large as 2 dB. In [30], 12 printed arc dipole units were used to achieve highly symmetric patterns, but the gain variations in the horizontal plane were still worse than 1.2 dB. On the contrary, the calibration loop antenna introduced in [31] had a good gain ripple around 0.2 dB, but its bandwidth was only 5%. To meet the calibration needs at frequencies from 400 MHz to 6 GHz, many such antennas with different working bands would be needed. Besides, for dipole-based narrowband antennas [31], reducing the ripples of the antenna design and suppressing the common mode currents simultaneously within the operating bandwidth is very challenging, which may result in a longer design cycle.

In this article, a small ripple, low cross polarization, and wide bandwidth calibration loop antenna is proposed, which consists of four arc-folded dipoles. This curved arc structure not only is small (with dimensions of $0.39\lambda_L \times 0.39\lambda_L \times 0.01\lambda_L$), but also achieves better omnidirectional property in the horizontal plane. This compact structure is further enhanced by adding parasitic strips. The proposed calibration loop antenna has achieved in the horizontal plane a small gain variation of no more than 0.16 dB as well as a bandwidth of 18% with $S_{11} < -10$ dB from 2.25 to 2.7 GHz. Besides, the proposed calibration loop antenna is a self-balanced antenna, which has less common mode current on the cable. By using balun structures, the proposed calibration loop antenna can suppress the common mode current on the coaxial cable and has obtained a high cross-polarization ratio. Thus, it is a suitable choice for the HP CA for MPAMS.

II. ANTENNA GEOMETRY AND DESIGN

A. Structure of the Proposed Antenna

Fig. 3 illustrates the geometry of the proposed calibration loop antenna. The antenna consists of four pairs of arc-shaped folded dipoles printed in an F4B ($\varepsilon_r = 2.65$ and $\tan \delta = 0.005$) board with a thickness of 1 mm. These dipoles are small in size with dimensions of $0.39\lambda_L \times 0.39\lambda_L \times 0.01\lambda_L$ only. The top surface details are shown in Fig. 3(a). The four embowed radiators are placed in a clockwise manner. They are connected to four parallel strip lines that terminated with a small circular conducting patch located in the center of the board. The small circular conducting patch is connected with the inner conductor of the coaxial cable acting as the feeding structure. On the edge of the board, four parasitic strips with the width of $w3$ are used for impedance matching. Two plating vias are used at the beginning of each radiator for ground connection.

The geometrical details of the bottom plane are shown in Fig. 3(b). Unlike that on the top plane, each arc-shaped folded dipole has two slots with different widths at the two ends. In addition, the strip connecting the dipole and the feed has multiple widths and the small circular
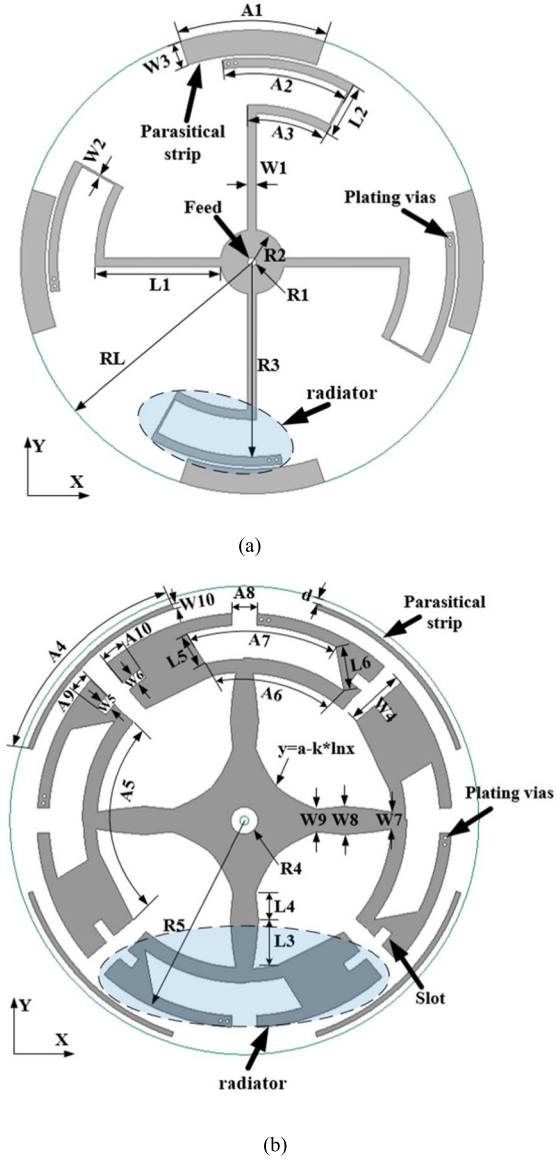
(a)

Fig. 3. Geometry of the proposed antenna. (a) Top plane. (b) Ground plane. $RL = 26$ mm, $R1 = 0.5$ mm, $R2 = 3.6$ mm, $R3 = 21.85$ mm, $R4 = 1.5$ mm, $R5 = 23$ mm, $A1 = 35°$, $A2 = 38°$, $A3 = 30.65°$, $A4 = 53.21°$, $A5 = 82.11°$, $A6 = 48.12°$, $A7 = 50.52°$, $A8 = 14°$, $A9 = 4.55°$, $A10 = 6.73°$, $L1 = 14.12$ mm, $L2 = 6.21$ mm, $L3 = 5.36$ mm, $L4 = 3.56$ mm, $L5 = 4$ mm, $L6 = 5$ mm, $W1 = 1$ mm, $W2 = 0.2$ mm, $W3 = 2.87$ mm, $W4 = 7.25$ mm, $W5 = 1.29$ mm, $W6 = 1.07$ mm, $W7 = 1.96$ mm, $W8 = 3.17$ mm, $W9 = 2.5$ mm, $W10 = 0.54$ mm, $d = 0.55$ mm, $a = 7.74$ mm, and $k = 3.12$ mm.

conducting patch in the center is replaced by a larger curved balun for the purpose of suppressing the common mode current.

B. Low Ripple Design

Engaging multiple radiators arranged in a circle to obtain a uniform current is a preferred implementation of omnidirectional antennas. The classic cloverleaf antenna introduced in [24] connects the four smaller rings to the coaxial cable to achieve a uniform loop current. The triangular loop antenna proposed in [32] has omni-directionality by employing three folded dipoles. If the length of the dipole is less than half of the wavelength, they will have the same current directions,
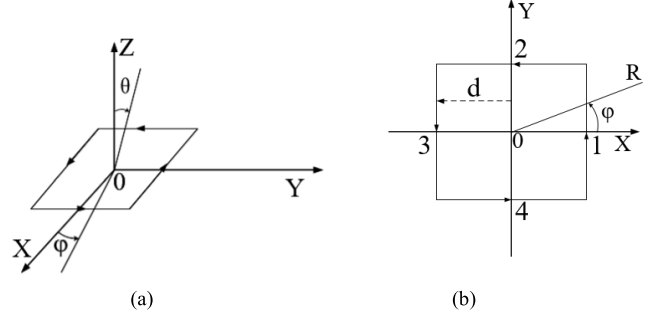

Fig. 4. Square ring array. (a) 3-D mode. (b) xoy plane.

and the current amplitude is approximately sinusoidal. It is well known that increasing the number of radiators can obtain an approximately uniform current distribution [33]. However, the increasing number of radiators makes the antenna larger and the impedance matching more difficult [34]. In order to have a compact size as well as a wideband, four folded dipoles are used in this article for the proposed calibration loop antenna.

Since the current distribution on the radiating element is not uniform, we need to study how we can achieve a low gain variation in the far-field of the combined array, so as to provide an initial value for the design of the calibration loop antenna. In order to better understand the physical concept of the combined array, we ignored the coupling between the arrays and used the square matrix composed of four short dipoles to simplify the complex model.

As shown in Fig. 4, a square ring array is placed in the center of the xoy plane. Four vertical short dipoles are located at the centers of the square edges. According to the antenna theory, in the dipole's coordinate system, the electric field generated by a vertical short dipole in the far-field is given by

$$E_\theta = j \frac{IL}{2\lambda r} \eta \sin\theta e^{-j\beta r} \tag{1}$$

where I is the current amplitude, L is the length of the radiator, λ is the wavelength, r is the distance from the antenna center to the observation point, η is the intrinsic impedance of media, β is the propagation constant, and θ is the angle between the antenna axis and the observation point.

Thus, the results of radiation fields generated by the short dipoles on the square ring array in the xoy plane can be obtained by coordinate transformation, as shown in Fig. 4, where R is the distance from the far-field observation point to the center of the square ring array; d is the distance from the short dipole to the center of the square ring $(R \gg d)$; φ is the angle between the projection in the xoy plane of the line from the far-field observation point to the center of the square ring and the X-axis

$$E_{1\varphi} = j \frac{IL}{2\lambda R} \eta \cos\varphi e^{-j\beta(R-d\cos\varphi)} \tag{2}$$

$$E_{2\varphi} = j \frac{IL}{2\lambda R} \eta \sin\varphi e^{-j\beta(R-d\sin\varphi)} \tag{3}$$

$$E_{3\varphi} = -j \frac{IL}{2\lambda R} \eta \cos\varphi e^{-j\beta(R+d\cos\varphi)} \tag{4}$$

$$E_{4\varphi} = -j \frac{IL}{2\lambda R} \eta \sin\varphi e^{-j\beta(R+d\sin\varphi)}. \tag{5}$$
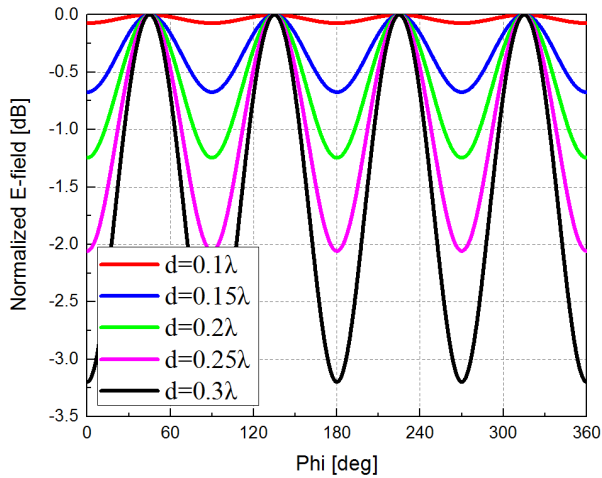
Fig. 5.   Normalized electric field with different d.

Without considering the mutual coupling, the far-field of the short dipole array in the *xoy* plane can be obtained as

$$E_{\text{square}\varphi} = E_{\varphi 1} + E_{\varphi 2} + E_{\varphi 3} + E_{\varphi 4}. \qquad (6)$$

After simplification, the array factor of the short dipole array in the *xoy* plane is

$$f(\varphi) = \cos\varphi \sin(\beta d \cos\varphi) + \sin\varphi \sin(\beta d \sin\varphi). \qquad (7)$$

According to (7), the pattern variation of the short dipole square ring array in the horizontal plane comes from the βd factor, where $\beta = 2\pi/\lambda$, and d represents the distance from each dipole element to the center of the square ring array. Thus, the pattern in the horizontal plane depends on the factor d/λ, which indicates that d is the key parameter in the square ring array that affects the ripple of the HP pattern.

Through MATLAB calculations, the normalized patterns of the short dipole square ring array in the horizontal plane are obtained with different values of d. As shown in Fig. 5, when $d \leq 0.3\ \lambda$, the smaller the distance d from each array element to the center of the square ring array, the smaller the ripple of the pattern in the horizontal plane. Unfortunately, because of the tapered current distribution of the short dipole, even when $d = 0.15\lambda$, the pattern variation of the square ring array in the horizontal plane is still larger than 0.7 dB. To obtain a more uniform current distribution, the four folded dipoles whose behavior can be described using (6) are curved in Fig. 6. In Fig. 6(a), the curved folded dipole is divided into two layers. The top layer of red is the feed layer and the bottom layer of blue is the ground plane. They are connected by plating vias. Fig. 6(b) compares the ground planes of the curved folded dipole and the folded dipole, which shows that the curved folded dipole has a smaller radius and more uniform current distribution. The simulated ripple of the curved folded dipoles at 2.5 GHz is shown in Fig. 8. Compared to the folded dipole square matrix without being curved, the curved one has a smaller gain variation in the horizontal plane less than 0.3 dB. However, since the curved folded dipoles just reduce the radius of the loop, the tapered current distribution of the dipole still exists.
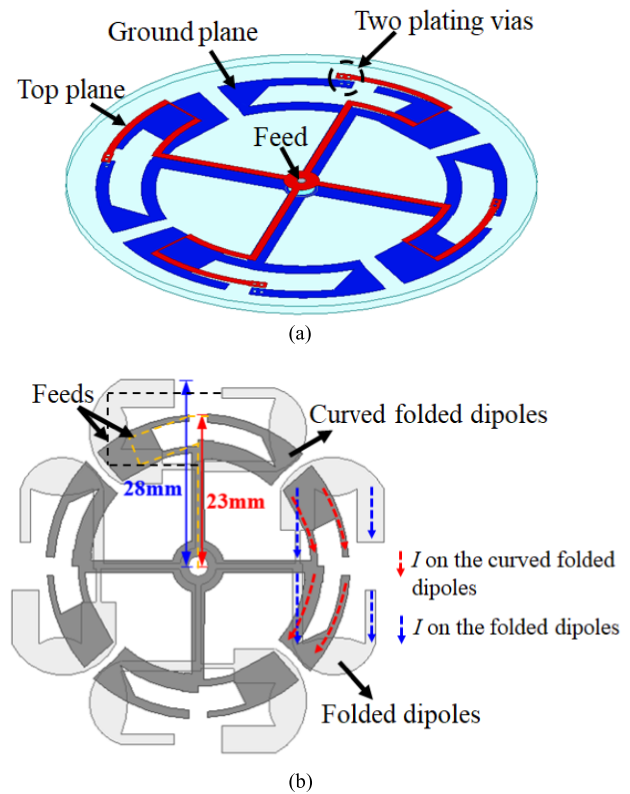

(a)

(b)

Fig. 6.   (a) Curved folded dipoles. (b) Comparison of folded dipoles and curved folded dipoles.
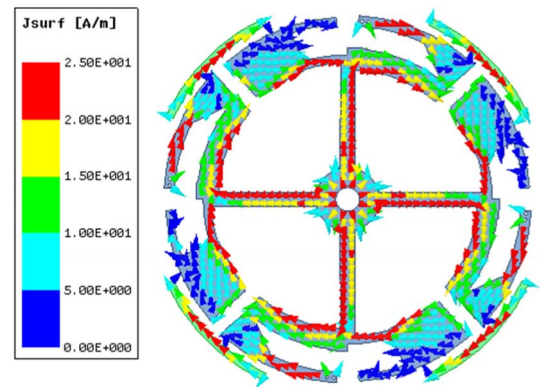

Fig. 7.   Current distribution of the curved folded dipoles with parasitic strips (bottom layer).

To solve this problem, four parasitic strips were added on the edge of the board. Fig. 7 shows the current distribution of the model. The current generated on the parasitic strips compensates for the weakened current at the end of the folded dipoles, enabling the antenna to have a more uniform current distribution.

Fig. 8 compares the ripples of different models. Obviously, the curved folded dipoles with parasitic strips have the smallest gain variation in the horizontal plane (less than 0.09 dB), which meets the CTIA standard.

C. Common-Mode Current Suppression

For the purpose of suppressing the common mode current, the proposed calibration loop antenna uses a voltage balun (also known as a natural balun) and a tapered balun.
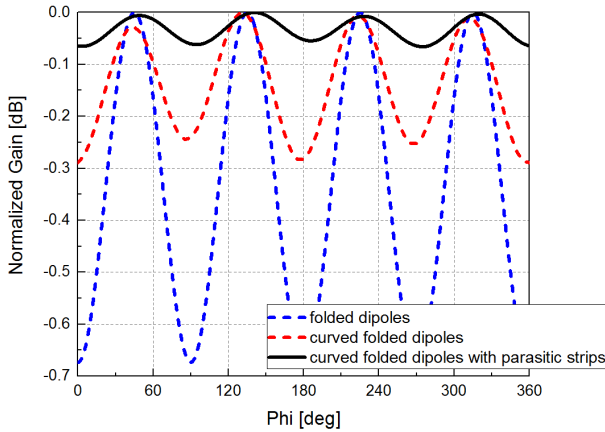
Fig. 8. Ripples of different models.

As illustrated in Fig. 9(a), the folded dipole is a natural balun that can make C point zero potential point [25]. Consequently, little current on the antenna will flow through the micro-strip line to the outside of the coaxial cable. Compared to a quarter-wavelength transmission line, this voltage-balanced structure is not limited by the frequency, so it has a wider bandwidth. The proposed calibration loop antenna used a micro-strip structure to implement the natural balun.

Since the natural balun can only suppress the common-mode current from radiators to the coaxial cable, some common-mode current on the coaxial cable arising from leakage of the field around the edge of the lower plate [36] still exists. In order to further eliminate the common mode current, an improved tapered balun was designed. As shown in Fig. 9(b), the tapered balun consists of two parts: part A to suppress the common mode current and part B to achieve impedance matching. The inner conductor of the coaxial cable is connected to the top layer in part A and the outer conductor is connected to the bottom ground layer in part A.

To analyze how part A suppresses the common mode current, its electric field distribution is drawn in Fig. 9(c). Notice that if the radius of the bottom area $R = \infty$, there is no current on the outer conductor of the coaxial cable [35]. Thus, controlling the ratio of R/r can make most of the electric field stay in the red region and only a small part of the fringing electric field can cross the bottom plane and land on the shield of the coaxial cable [35]. It can also be understood that only a small portion of the magnetic flux lines can wrap both planes and cause current on the backside of the bottom plane. This greatly reduces the current on the outer conductor of the coaxial cable. The bottom plane in part A further has symmetric tapered contour lines. Compared to the circular structure, the symmetric tapered contour lines allow for a better combination of part A and part B, which has better impedance matching. One of them can be described mathematically using the *xoy* coordinates as

$$y = a - k \ln x \qquad (8)$$

where a is 3.12 (unit: mm) and k is 7.74.

Part B of the tapered balun is used to achieve wideband impedance matching [35]. As a result, the strips were designed

into multiple segments with different widths on the bottom layer for different frequency bands.

Fig. 9(d) shows the simulated results of the cross-polarization ratio from 2.2 to 2.8 GHz. It is clear that the cross-polarization ratio in the operating band from 2.25 to 2.7 GHz is lower than -28 dB, after both the natural and tapered baluns are introduced. These results confirm that the proposed balun structures play an effective role in suppressing the common mode current in a wide bandwidth.

D. Bandwidth Enhancement

Four parasitic strips on both the top and bottom layers and etched slots on the bottom layer are introduced to enhance impedance matching in the desired frequency band. Fig. 10 compares the reflection coefficient of the proposed calibration loop antenna with and without the parasitic strips and the slots. The results show that the antenna with the slots has two resonances at lower and higher frequencies, which widens the bandwidth of the antenna. When adding the parasitic strips, the proposed calibration loop antenna has a lower reflection coefficient, $S_{11} < -15$ dB, in the band of 2.29–2.62 GHz (over 13% bandwidth). It is clear that the parasitic strips and the etched slots effectively change the impedance characteristics of the antenna.

III. EXPERIMENTAL RESULTS AND ANALYSIS

A. Measuring Environment

To validate the antenna performance, the proposed calibration loop antenna was fabricated on a low-cost, 1-mm-thick, F4B board with a permittivity of 2.65 and a loss tangent of 0.005 (measured at the frequency of 2.2–2.7 GHz). The top and bottom of the fabricated antenna are shown in Fig. 11. The compact antenna structure has dimensions of only $0.39\lambda_L \times 0.39\lambda_L \times 0.01\lambda_L$.

As shown in Fig. 12, the antenna was measured in a far-field antenna chamber, Dart 9000B by General Test System (GTS), which has a length of 11 m. The electromagnetic shielding effectiveness of this chamber is above 100 dB and the reflection level of the quiet zone is below -40 dB.

B. Radiation Properties

The simulated and measured radiation patterns in the *E*-plane (*xoy*) at 2.25, 2.45, 2.55, and 2.75 GHz of the proposed calibration loop antenna are compared in Fig. 13(a)–(d), respectively. A good agreement between simulations and measurements has been achieved. Furthermore, it is obvious that the proposed calibration loop antenna has an extremely small gain variation in the horizontal plane and low cross polarization over the working band.

C. Gain Variation

Fig. 14 further plots the simulated and measured gain variations in the *E*-plane over frequency. It can be seen that the proposed calibration loop antenna obtains a small gain variation less than 0.16 dB over 20% bandwidth. However, the measured results of gain variation are slightly different
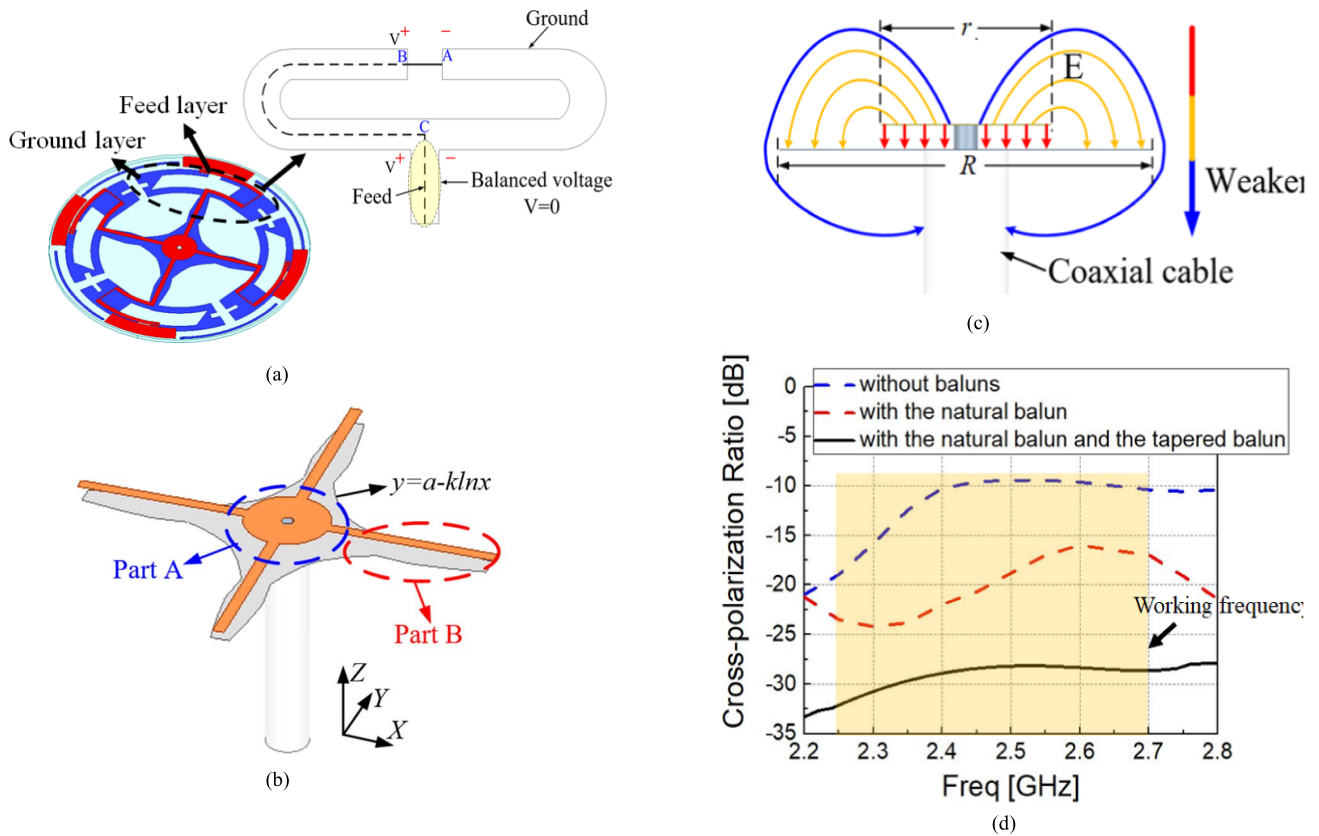
Fig. 9. (a) Principle of natural balun. (b) Tapered balun. (c) Principle of part A. (d) Simulated cross-polarization ratio.
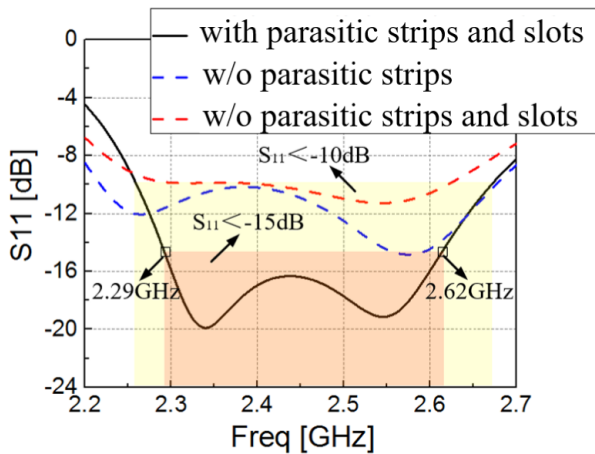

Fig. 10. Simulated $|S_{11}|$ of the proposed antenna with/without parasitic strips and slots.

Fig. 11. Fabricated antenna. (a) Top view. (b) Bottom view.

from the simulation results. There are several reasons for this: 1) reflections in the anechoic chamber may cause a ±0.1-dB uncertainty to the measured results [12]; 2) the errors caused by antenna manufacturing; 3) the limited accuracy of the turntables, rotary axes, etc. in the measurement chamber; 4) mechanical instability of the rotating joint; 5) uneven dielectricity of the fixtures; and 6) a little common mode current that exists on the coaxial cable. Despite this, the gain variation in the horizontal plane of the antenna is no more than 0.16 dB, which is in line with the requirements of the CTIA.
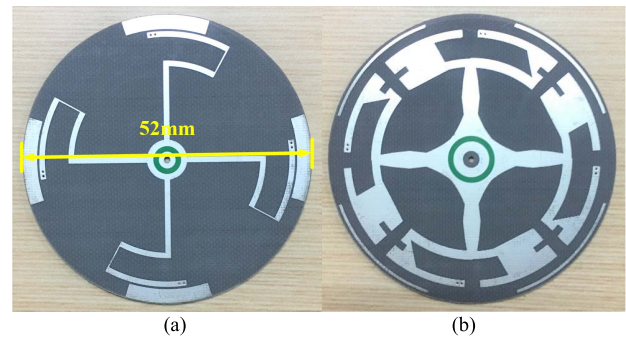
D. Common-Mode Current

The cross polarization of the proposed calibration loop antenna is primarily caused by radiation from the common mode current on the coaxial cable, which could severely affect the radiation properties of the antenna, resulting in calibration errors. From Fig. 15, the measured cross-polarization ratio from 2.25 to 2.75 GHz is greater than 24 dB, which demonstrates the effectiveness of the proposed baluns in common mode suppression.

However, being affected by the cross-polarization isolation of the measurement antenna in the antenna chamber together with other issues mentioned earlier, the measured results do not match perfectly with the simulated results.

In order to further check the effect of suppressing the common mode current, the gain ripple of the proposed

(a)
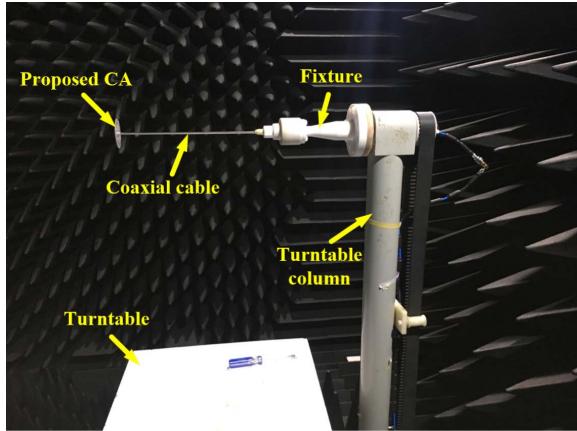
(b)

Fig. 12. Dart-9000 antenna chamber and measurement set-up. (a) Front view of the chamber. (b) Interior of the chamber.
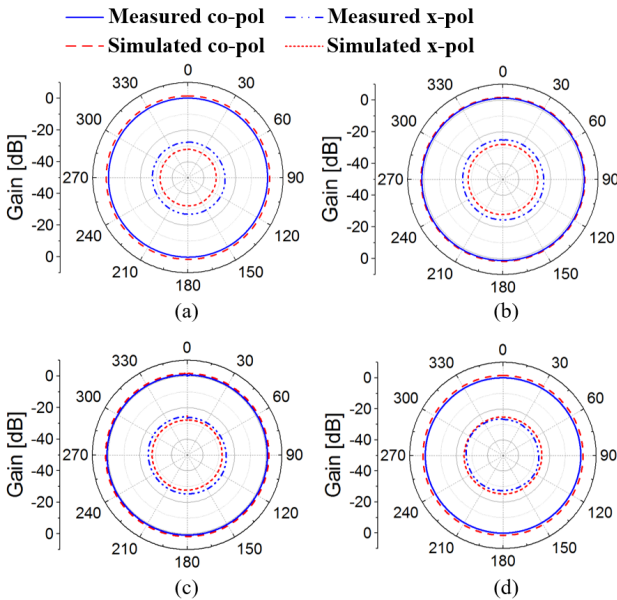

Fig. 13. Simulated and measured radiation patterns at (a) 2.25, (b) 2.45, (c) 2.55, and (d) 2.75 GHz.

calibration loop antenna with a bent coaxial cable was measured. As shown in Fig. 16, the distance between the bent coaxial cable and the calibration loop antenna is 30 cm. The measurement result is shown in Fig. 14; the gain ripple of the bent one is smaller than 0.15 dB, which shows that the proposed calibration loop antenna with a bent coaxial cable still
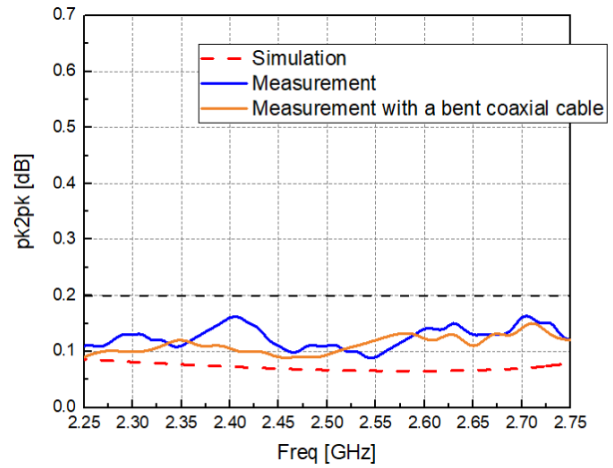
Fig. 14. Gain variation of the proposed CA over the work band.
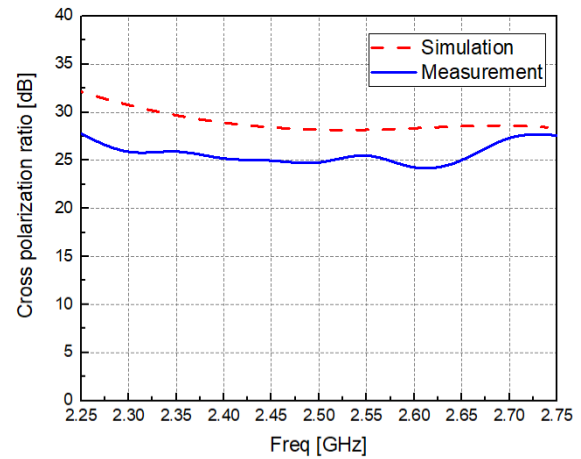
Fig. 15. Cross-polarization ratio of the proposed CA.

Fig. 16. Proposed CA with a bent coaxial cable.

has a good pattern symmetry performance. As referred earlier, there are slight differences between the two measurements.

E. Reflection Coefficient

Obtained from a vector network analyzer, N5230AC from Keysight, the measured reflection coefficient shows a good performance of below −10 dB in the 2.25–2.7 GHz range, about 18% bandwidth, and below −15 dB in 13% bandwidth,

TABLE I

COMPARISON OF THE PROPOSED ANTENNA AND OTHER LOOP ANTENNAS

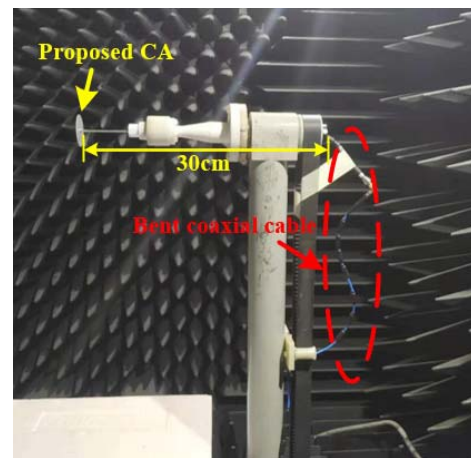| Reference Designs	Operating Freq. (GHz)	Antenna size (mm³) (λ_L at the lowest frequency)	Gain variation (dB)	Cross polarization ratio (dB)
Ref. [22]	5.1-6.8	$48.4 \times 48.4 \times 1$ ($0.82\lambda_L \times 0.82\lambda_L \times 0.01\lambda_L$)	3	10
Ref. [26]	1.25-7.6	$176 \times 176 \times 1$ ($0.73\lambda_L \times 0.73\lambda_L \times 0.01\lambda_L$)	1.5	23
Ref. [28]	1.85-3.88	$120 \times 120 \times 1$ ($0.63\lambda_L \times 0.63\lambda_L \times 0.01\lambda_L$)	2.2	23
Ref. [29]	1.19-2.0	$85 \times 85 \times 26.7$ ($0.34\lambda_L \times 0.34\lambda_L \times 0.11\lambda_L$)	2	20
Ref. [30]	1.7-3.2	$150 \times 150 \times 1$ ($0.85\lambda_L \times 0.85\lambda_L \times 0.01\lambda_L$)	1.2	15
Ref. [31]	2.4-2.53	$52.4 \times 52.4 \times 1$ ($0.42\lambda_L \times 0.42\lambda_L \times 0.01\lambda_L$)	0.2	20
This work	2.25-2.7	$52 \times 52 \times 1$ ($0.39\lambda_L \times 0.39\lambda_L \times 0.01\lambda_L$)	0.16	24
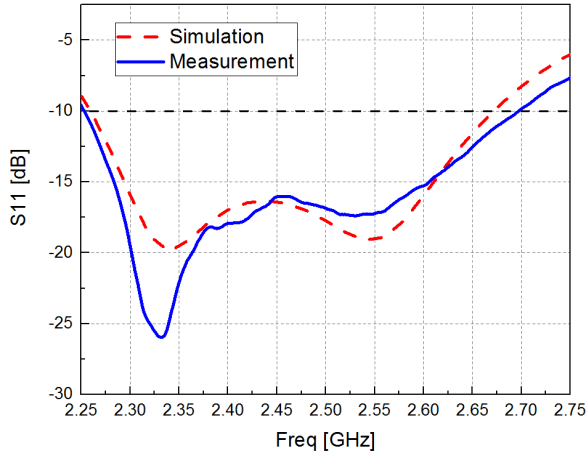
Fig. 17. Reflection coefficient.

as shown in Fig. 17. The measured results show good correlation with the simulated results.

F. Comparison With Other HP Omnidirectional Antennas

The comparisons between the proposed calibration loop antenna and other loop antennas, in terms of operating frequency, antenna dimensions, gain variations, and cross-polarization ratio, are listed in Table I. Apparently, the antenna in [26] had a wide bandwidth, but its size was as large as $0.73\lambda_L$. Although the antenna in [29] achieved a small size, its gain variation was worse than 2 dB. In [31], the antenna obtained a highly symmetric pattern, but its bandwidth was only 5%. The proposed calibration loop antenna, on the other hand, achieved good performance in all these aspects: a small gain variation, a good cross-polarization ratio, and a small size in a wide bandwidth.

IV. CONCLUSION

Composed of four arc-folded dipoles, a compact calibration loop antenna with small gain ripple and low cross polarization is proposed in this article. Utilizing both the natural and tapered balun structures not only achieves a small antenna with dimensions of $0.39\lambda_L \times 0.39\lambda_L \times 0.01\lambda_L$, but also effectively suppresses the common mode current. The measured results indicate that the proposed calibration loop antenna has a 10-dB return loss bandwidth from 2.25 to 2.7 GHz. Within the operating bandwidth, the gain variation in the horizontal plane

is less than 0.16 dB and the cross-polarization ratio is greater than 24 dB. Due to this excellent performance, the proposed calibration loop antenna is very suitable to be used in the calibration of anechoic chambers, especially for those small-sized, multiprobe ones.

REFERENCES

[1] Y. Qi et al., "5G over-the-air measurement challenges: Overview," IEEE Trans. Electromagn. Compat., vol. 59, no. 6, pp. 1661–1670, Dec. 2017.

[2] P. Shen, Y. Qi, W. Yu, F. Li, and J. Fan, "Fast and accurate TIS testing method for wireless user equipment with RSS reporting," IEEE Trans. Electromagn. Compat., vol. 58, no. 3, pp. 887–895, Jun. 2016.

[3] X. Chen, W. Fan, L. Hentila, P. Kyosti, and G. F. Pedersen, "Throughput modeling and validations for MIMO-OTA testing with arbitrary multi-path," IEEE Antennas Wireless Propag. Lett., vol. 17, no. 4, pp. 637–640, Apr. 2018.

[4] I. C. Llorente, W. Fan, and G. F. Pedersen, "MIMO OTA testing in small multiprobe anechoic chamber setups," IEEE Antennas Wireless Propag. Lett., vol. 15, pp. 1167–1170, 2016.

[5] W. Fan et al., "Antenna pattern impact on MIMO OTA testing," IEEE Trans. Antennas Propag., vol. 61, no. 11, pp. 5714–5723, Nov. 2013.

[6] L. J. Foged, G. Barone, and F. Saccardi, "Antenna measurement systems using multi-probe technology," in Proc. IEEE Conf. Antenna Meas. Appl. (CAMA), Nov. 2015, pp. 1–3.

[7] Y. Jing, H. Kong, and M. Rumney, "MIMO OTA test for a mobile station performance evaluation," IEEE Instrum. Meas. Mag., vol. 19, no. 3, pp. 43–50, Jun. 2016.

[8] P. Shen, Y. Qi, W. Yu, J. Fan, and F. Li, "OTA measurement for IoT wireless device performance evaluation: Challenges and solutions," IEEE Internet Things J., vol. 6, no. 1, pp. 1223–1237, Feb. 2019.

[9] H. Garn, M. Buchmayr, W. Mullner, and J. Rasinger, "Primary standards for antenna factor calibration in the frequency range of (30 to 1000) MHz," IEEE Trans. Instrum. Meas., vol. 46, no. 2, pp. 544–548, Apr. 1997.

[10] W. Stutzman and G. Thiele, Antenna Theory and Design. Hoboken, NJ, USA: Wiley, 2013.

[11] M. Ishii and Y. Shimada, "Reference calibration methods for small circular loop antenna in low-frequency band," IEEE Trans. Instrum. Meas., vol. 58, no. 4, pp. 1097–1103, Apr. 2009.

[12] Test Plan for 2×2 Downlink MIMO and Transmit Diversity Over-the-Air Performance, Revision 1.1, Telecommun. Internet Assoc., Washington, DC, USA, Aug. 2016.

[13] C. Icheln, J. Krogerus, and P. Vainikainen, "Use of balun chokes in small-antenna radiation measurements," IEEE Trans. Instrum. Meas., vol. 53, no. 2, pp. 498–506, Apr. 2004.

[14] Z. Chen, N. Yang, Y.-X. Guo, and M. Chia, "An investigation into measurement of handset antennas," IEEE Trans. Instrum. Meas., vol. 54, no. 3, pp. 1100–1110, Jun. 2005.

[15] A. Vorobyov, J. Zijderfeld, A. Yarovoy, and L. Ligthart, "Impact common mode currents on miniaturized UWB antenna performance," in Proc. Eur. Microw. Conf., 2005, pp. 285–288.

[16] A. Alford and A. G. Kandoian, "Ultrahigh-frequency loop antennas," Electr. Eng., vol. 59, no. 12, pp. 843–848, Dec. 1940.

[17] H. Nakano, R. Satake, and J. Yamauchi, "Horizontally polarized, omni-directional antenna with a single feed," in Proc. IEEE Int. Conf. Wireless Inf. Technol. Syst., Aug. 2010, pp. 1–4,.

[18] C.-C. Lin, L.-C. Kuo, and H.-R. Chuang, "A horizontally polarized omnidirectional printed antenna for WLAN applications," *IEEE Trans. Antennas Propag.*, vol. 54, no. 11, pp. 3551–3556, Nov. 2006.

[19] C.-H. Ahn, S.-W. Oh, and K. Chang, "A dual–frequency omnidirectional antenna for polarization diversity of MIMO and wireless communication applications," *IEEE Antennas Wireless Propag. Lett.*, vol. 8, pp. 966–969, 2009.

[20] B. Qun Wu and K.-M. Luk, "A wideband, low-profile, conical-beam antenna with horizontal polarization for indoor wireless communications," *IEEE Antennas Wireless Propag. Lett.*, vol. 8, pp. 634–636, 2009.

[21] J. Morrow, "Polarization-adjustable omnidirectional dipole array," *IEEE Antennas Wireless Propag. Lett.*, vol. 2, pp. 223–225, 2003.

[22] G. G. Zhang, H. Zhang, Z. L. Yuan, Z. M. Wang, and D. Wang, "A novel broadband E-plane omni–directional planar antenna," *J. Electromagn. Waves Appl.*, vol. 24, nos. 5–6, pp. 663–670, Jan. 2010.

[23] K. Wei, Z. Zhang, Z. Feng, and M. F. Iskander, "A MNG-TL loop antenna array with horizontally polarized omnidirectional patterns," *IEEE Trans. Antennas Propag.*, vol. 60, no. 6, pp. 2702–2710, Jun. 2012.

[24] P. H. Smith, "'Cloverleaf' antenna for F.M. broadcasting," *Proc. IRE*, vol. 35, no. 12, pp. 556–1563, 1947.

[25] J. D. Kraus and R. J. Marhefka, *Antennas For All Applications*, 3rd ed. 2013, p. 235.

[26] H. Liu, Y. Liu, W. Zhang, and S. Gao, "An ultra-wideband horizontally polarized omnidirectional circular connected vivaldi antenna array," *IEEE Trans. Antennas Propag.*, vol. 65, no. 8, pp. 4351–4356, Aug. 2017.

[27] Y. Yu and F. Jolani, "A wideband omnidirectional horizontally polarized antenna for 4G LTE applications," *IEEE Antennas Wireless Propag. Lett.*, vol. 12, pp. 686–689, 2013.

[28] H.-Y. Zhang, F.-S. Zhang, F. Zhang, T. Li, and C. Li, "Bandwidth enhancement of a horizontally polarized omnidirectional antenna by adding parasitic strips," *IEEE Antennas Wireless Propag. Lett.*, vol. 16, pp. 880–883, 2017.

[29] X. Cai and K. Sarabandi, "A compact broadband horizontally polarized omnidirectional antenna using planar folded dipole elements," *IEEE Trans. Antennas Propag.*, vol. 64, no. 2, pp. 414–422, Feb. 2016.

[30] Z. Wang and Y. Yin, "Design of a wideband horizontally polarized omnidirectional antenna with mutual coupling method," *IEEE Trans. Antennas Propag.*, vol. 63, no. 7, pp. 3311–3316, Jul. 2015.

[31] M. Chao, W. He, W. Yu, and Y. Qi, "Horizontally polarized antenna for calibration of a multiple probe antennas measurement system," *IEEE Trans. Electromagn. Compat.*, to be published.

[32] A. G. Kandoian and R. A. Felsenheld, "Triangular high-band TV loop antenna system," *Communications*, vol. 29, pp. 16–18, Aug. 1949.

[33] D. Rodrigo, L. Jofre, and B. A. Cetiner, "Circular beam-steering reconfigurable antenna with liquid metal parasitics," *IEEE Trans. Antennas Propag.*, vol. 60, no. 4, pp. 1796–1802, Apr. 2012.

[34] M. Gans and D. Kajfez, "Frequency independent baluns," *Proc. IEEE*, vol. 53, no. 6, pp. 647–648, Jun. 1965.

[35] R. E. Collin, "The optimum tapered transmission line matching section," *Proc. IRE*, vol. 44, no. 4, pp. 539–548, 1956.

Yihong Qi (Senior Member, IEEE) received the B.S. degree in electronics from the National University of Defense Technologies, Changsha, China, in 1982, the M.S. degree in electronics from the Chinese Academy of Space Technology, Beijing, China, in 1985, and the Ph.D. degree in electronics from Xidian University, Xi'an, China, in 1989.

From 1989 to 1993, he was a Post-Doctoral Fellow and then an Associate Professor with Southeast University, Nanjing, China. From 1993 to 1995, he was a Post-Doctoral Researcher with McMaster University, Hamilton, ON, Canada. From 1995 to 2010, he was with Research in Motion (Blackberry), Waterloo, ON, Canada, where he was the Director of Advanced Electromagnetic Research. He is currently a Scientist with the Peng Cheng Laboratory, Shenzhen, China, and the President and the Chief Scientist with General Test Systems, Inc., Shenzhen. He founded DBJay in 2011. He is also an Adjunct Professor with the EMC Laboratory, Missouri University of Science and Technology, Rolla, MO, USA, and Western University, London, ON, an Honorary Professor with Southwest Jiaotong University, Chengdu, China, and an Adjunct Professor with Hunan University, Changsha. He is an inventor of more than 450 published and pending patents.

Dr. Qi is a fellow of the Canadian Academy of Engineering and the National Academy of Inventors. He received the IEEE EMC Society Technical Achievement Award in August 2017. He was a Distinguished Lecturer of the IEEE EMC Society from 2014 to 2015 and the Founding Chairman of the IEEE EMC TC-12.

Yuming Zheng (Student Member, IEEE) received the B.S. degree in electronic information and technology from Hunan Normal University, Changsha, China, in 2016. He is currently pursuing the M.Sc. degree with the College of Electronic Information and Technology, Hunan University, Changsha.

His research interests include omnidirectional antennas, calibration for anechoic chambers, and antenna measurements.

Jun Fan (Fellow, IEEE) received the B.S. and M.S. degrees in electrical engineering from Tsinghua University, Beijing, China, in 1994 and 1997, respectively, and the Ph.D. degree in electrical engineering from the University of Missouri–Rolla, Rolla, MO, USA, in 2000.

From 2000 to 2007, he was a Consultant Engineer with NCR Corporation, San Diego, CA, USA. In July 2007, he joined the Missouri University of Science and Technology (formerly University of Missouri–Rolla), where he is currently an Associate Professor with the Missouri S&T Electromagnetic Compatibility (EMC) Laboratory. His current research interests include signal integrity and electromagnetic interference (EMI) designs in high-speed digital systems, dc power-bus modeling, intersystem EMI and radio frequency interference, printed circuit board noise reduction, differential signaling, and cable/connector designs.

Dr. Fan received the IEEE EMC Society Technical Achievement Award in August 2009. He was the Chair of the IEEE EMC Society's TC-9 Computational Electromagnetics Committee from 2006 to 2008 and was a Distinguished Lecturer of the IEEE EMC Society from 2007 to 2008. He is also the Vice Chair of the Technical Advisory Committee of the IEEE EMC Society. He is also an Associate Editor of the IEEE TRANSACTIONS ON ELECTROMAGNETIC COMPATIBILITY and the EMC Magazine.

Zibin Weng (Member, IEEE) received the B.S. degree in electronic engineering and the Ph.D. degree in electromagnetic field and microwave technology from Xidian University, Xi'an, China, in 2004 and 2009, respectively.
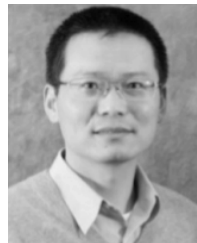
He is currently an Associate Professor with Xidian University. His current research interests include circularly polarized antennas, millimeter-wave antennas, and antenna arrays.

Fuhai Li (Member, IEEE) received the B.S. and M.S. degrees in instrument science and technology from Hunan University, Changsha, China.

He was a Professor with Hunan University. During his tenure, he had several science and technology progress awards. His students had lots of awards in kinds of national competitions under his leadership. He had published more than 22 articles in the national core journals and involved the compiling of university teaching materials.
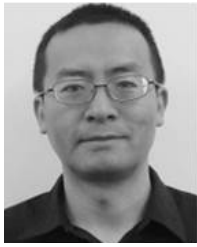
Zhiping Yang (Senior Member, IEEE) received the B.S. and M.S. degrees in electrical engineering from Tsinghua University, Beijing, China, in 1994 and 1997, respectively, and the Ph.D. degree in electrical engineering from the University of Missouri–Rolla, Rolla, MO, USA, in 2000.

From 2000 to 2005, he worked as a Technical Leader with Cisco Systems, San Jose, CA, USA. From 2005 to 2006, he worked as a Principal Engineer with Apple Computer, Cupertino, CA. From 2006 to 2012, he worked as a Principal Engineer with Nuova Systems (which was acquired by Cisco in 2008) and Cisco Systems, San Jose. From 2012 to 2015, he worked as a Senior Manager with Apple, Cupertino. He is currently a Senior Hardware Manager with the Google's Consumer Hardware Group, Mountain View, CA. He has published more than 40 research articles and 17 patents. His research and patents have been applied in Google Chromebook, Apple iPhone 5S/6/6S, Cisco UCS, Cisco Nexus 6 K/4 K/3 K, and Cisco Cat6K products. His research interests include signal integrity and power integrity methodology development for die/package/board codesign, high-speed optical module, various high-speed cabling solution, high-speed dynamic random access memory/storage technology, high-speed serial signal ingtechnology, and RF interference.

Dr. Yang was a recipient of the 2016 IEEE EMCS Technical Achievement Award.

James L. Drewniak (Fellow, IEEE) received the B.S., M.S., and Ph.D. degrees in electrical engineering from the University of Illinois at Urbana–Champaign, Champaign, IL, USA, in 1985, 1987, and 1991, respectively.

He is currently with the Electromagnetic Compatibility Laboratory, Department of Electrical and Computer Engineering, Missouri University of Science and Technology, Rolla, MO, USA. His research is in electromagnetic compatibility, signal and power integrity, and electronic packaging.